analytical chemistry

pubs.acs.org/ac Article

Programmable DNA Tweezer-Actuated SERS Probe for the Sensitive Detection of AFB_1

Jinjie Li,[§] Wenjing Wang,[§] Hao Zhang, Zhicheng Lu, Wenxin Wu, Mingbo Shu, and Heyou Han*

Cite This: *Anal. Chem.* 2020, 92, 4900−4907 Read Online

ACCESS | Metrics & More | Article Recommendations | Supporting Information

ABSTRACT: A DNA tweezer is a dynamic DNA nanomachine that can reversibly switch its state between open and closed. Here, we employed a DNA tweezer for the first time to dynamically control the distance between plasmonic silver nanoparticles (Ag NPs) for a surface enhanced Raman scattering (SERS) biosensing application. Two DNA and 4-nitrothiophenol (4-NTP) modified Ag NPs were linked to the arms of the DNA tweezer (DNA tweezer-Ag NPs probe) by complementary base pairing. Activation of the Raman intensity was achieved by the state transformation of the DNA tweezer-Ag NPs probe from open to closed. The distances between two Ag NPs in open and closed state were 8.1 ± 2.7 nm and 3.2 ± 0.8 nm, respectively. Furthermore, the two Ag NPs were spatially separated in the open state with a low Raman signal, whereas in the closed state, Raman intensity was enhanced because of the proximity of two Ag NPs. The developed biosensing system exhibited a good linear relationship when the concentration of aflatoxin B_1 (AFB_1) ranged from 1 ng/mL to 0.01 pg/mL, and the limit of detection (LOD) was 5.07 fg/mL. In addition, spike recovery and certificated real foodstuffs were used to examine the feasibility in a real situation. This protocol provides a potential candidate for SERS detection and can be used as a promising technology for biological and chemical sensors.

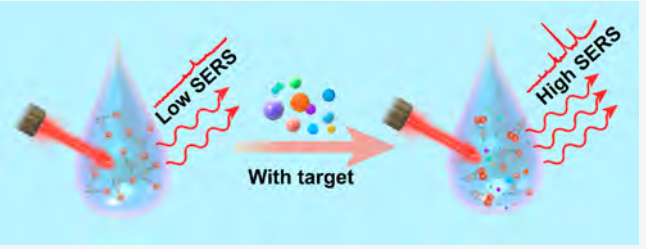

DNA nanotechnology starts from using DNA as building blocks to construct nanoscale patterns, which is termed as structural DNA nanotechnology.[1] One of the milestones in this area is DNA origami first proposed by Rothemund in 2006.[2] Folding a long single-stranded staple DNA with multiple staple strands into precisely defined nanostructures can be realized in one-step annealing with high yield. Because of the site-specific addressability of staple strands, nanoparticles can be arranged at the interface of DNA origami with nanoscale accuracy.[3] Light can be focused in subwavelength volumes by these DNA origami-oriented plasmonic nanostructures, leading to significantly enhanced local fields.[4,5] Surface enhanced Raman scattering (SERS) is a novel spectroscopy technique with unique properties.[6−8] Compared with fluorescence spectroscopy, SERS are less prone to photobleaching allowing for longer observation and have spectral fingerprinting for multiplex detection.[9−11] At the same time, SERS can enable single-molecule detection.[12] These advantages make SERS widely used in analytical,[13−15] biomedical,[16] and physical chemistry.[17] The hot spot provided by the adjacent plasmonic nanoparticles holds great promise in SERS applications.[18−24] For example, a single streptavidin protein molecule labeled with alkyne groups was placed in the gap of silver nanolenses with the highest electric field enhancement, and the SERS signals of alkyne groups from a single protein were detected using the cascaded enhancement mechanism.[25] The SERS signal of static positioned molecule between two DNA origami-oriented plasmonic nanoparticles has been studied as presented above, while plasmonic nanoparticles with a tunable distance controlled by DNA nanotechnology for SERS biosensing applications has never been explored before.

A DNA tweezer is a dynamic DNA nanodevice that can reversibly switch its state between open and closed by adding DNA fuel strands.[26] By modifying fluorescent molecules at specific tweezer arms, fluorescence resonance energy transfer can be clearly observed when operating the DNA tweezers. On the basis of this finding, a series of biosensing applications including microRNA,[27] gene[28] and protein analysis,[29] and pH monitoring[30] have been demonstrated. Interestingly, a DNA tweezer was reported to precisely tune the distance between the enzyme and cofactor which is modified at tweezer arms, leading to an enzyme nanoreactor to regulate the biofunction of the enzyme.[31] Similarly, an enzyme cascade reaction was reported to be dynamically regulated by a DNA tweezer as well,[32] and a biosensing application has been presented on the basis of this principle.[33] Inspired by the above results, we speculate a DNA tweezer can be used to tune the distance between nanoparticles for wider applications.

Received: October 22, 2019
Accepted: March 8, 2020
Published: March 8, 2020

https://dx.doi.org/10.1021/acs.analchem.9b04822
Anal. Chem. 2020, 92, 4900−4907

In this work, we employed a DNA tweezer for the first time to dynamically control the distance between plasmonic silver nanoparticles (Ag NPs) for a SERS biosensing application. Aflatoxin B_1 (AFB_1) was chosen as the target model considering its severe toxicity and carcinogenicity to humans and animals.[34,35] We incorporated AFB_1 aptamer into the DNA tweezer by partially DNA hybridization to accommodate the open state. Ag NPs were modified at two arms of DNA tweezer using Ag−S chemistry forming DNA tweezer-actuated SERS probes.[36−38] Two Ag NPs were speculated to be separated at open state, which showed a negligible enhancement of SERS signal.[14,32,39−42] In the presence of the AFB_1 target, the unhybridized overhang of AFB_1 aptamer tended to bind with the analytes, releasing aptamer from DNA tweezer to generate a closed state. Accordingly, two Ag NPs approached each other to exhibit a closer distance, thus showing a significantly enhanced SERS signal to indicate the presence of target. Additionally, we also demonstrated the feasibility to detect oligonucleotide using the proposed DNA tweezer-actuated SERS probes, indicating their programmability and versatility for sensitive detection of a variety of targets.

EXPERIMENTAL SECTION

Chemical Reagents. All the DNA oligonucleotides utilized in this study were synthesized and purified by Sangon Biotech Co., Ltd. (Shanghai, China), and all the DNA sequences are listed in Table S1. Commercial nucleic acid staining dye (10000×) was purchased from Yisheng Biotechnolgy Co., Ltd. (Shanghai, China). Aflatoxin B_1 (AFB_1), aflatoxin B_2 (AFB_2), aflatoxin G_1 (AFG_1), aflatoxin G_2 (AFG_2), aflatoxin M_1 (AFM_1), zearalenone (ZON), and deoxynivalenol (DON) were supplied by Sigma-Aldrich Trading Co., Ltd. (Shanghai, China). Silver nitrate ($AgNO_3$), trisodium citrate (TSC), sodium borohydride ($NaBH_4$), Tris, acetic acid, ethylenediaminetetraacetic acid (EDTA), magnesium acetate, 4-nitrothiophenol (4-NTP), and other chemicals with analytical grade were supplied by Sinopharm Chemical Reagent Co., Ltd. (Shanghai, China). Tris(2-carboxyethyl)-phosphin hydrochloride (TCEP) and agarose B with low electroosmosis (biotech grade) were purchased from Sangon Biotech Co., Ltd. (Shanghai, China). The samples was prepared using water purified by a Milli-Q system (resistivity of 18.2 MΩ cm). All the glassware and magnetic stirring bars used in this work were soaked in freshly prepared aqua regia [$HCl:HNO_3$ = 3:1(v/v)] overnight and then rinsed thoroughly with ultrapure water.

Apparatus. Raman spectra was carried out using an inVia Raman spectrometer (Renishaw, UK) with a 633 nm He−Ne laser and 10 mW laser power. UV−vis absorption spectra was performed by a UV−vis spectrometer (TU-1901, Beijing Purkinje General Instrument Co., Ltd.). Transmission electron microscopy (TEM) images were captured by a JEM-2010 transmission electron microscope (JEOL, Japan). Hydrodynamic diameters of nanoparticles were measured by Zetasizer Nano ZS90 DLS system (Malvern, England). Gel images were captured using a ChemiDoc Touch Imaging System from Bio-Rad Laboratories (Bio-Rad Laboratories, Hercules, Canada). The fluorescence spectra were monitored with a RF-5301PC fluorescence spectrophotometer (Shimadzu Corp., Tokyo, Japan). The excitation of 5-carboxyfluorescein (FAM) was performed at 495 nm, and the emission was recorded at 520 nm. Atomic force microscope (AFM) imaging was performed with a standard AFM instrument (Multimode 8 microscope, Bruker) using silicon probes (SNL-10, Bruker) with a nominal resonance frequency of ∼28 kHz and a stiffness of 0.12 N/m.

Preparation of Ag Nanoparticles (Ag NPs). Ag NPs with a diameter of approximately 10 nm were synthesized according to the method mentioned by Lee-Meisel's method with slight modifications.[43] Briefly, 100 mL of 1 mM $AgNO_3$ aqueous solution was stirred vigorously until boiling. Subsequently, 2 mL of 1 wt % TSC was added in one quick motion. After that, a portion of 300 μL of freshly prepared ice-cold 3 mM $NaBH_4$ solution was added to the above-mentioned mixture immediately, leading to a color change from colorless to yellowish. The solution was kept boiling for another 15 min to finish the reduction, and then the prepared Ag NPs was cooled to room temperature and stored at 4 °C for subsequent experiments.

Functionalization of Ag NPs with SH-DNA and Raman Reporter. DNA-functionalized Ag NPs were prepared using a modified salt-aging method as that described in a literature procedure.[44] The thiol-DNAs were modified on the surface of the Ag NPs through Ag−S covalent bonds.[45] The conjugation process was carried out as follows: first, TCEP was used to reduce the intramolecular disulfide bond in SH-DNA at a stoichiometric ratio of 100:1 in acetate buffer (pH = 5.2) at 37 °C for 1 h. Then Ag NPs and SH-DNA were incubated in a stoichiometric ratio of 1:300 at 4 °C. After incubation for 16 h, the mixture was salted with 100 mM NaCl by adding 5 M NaCl in three times and incubated for another 24 h at 4 °C. After that, the Raman reporter (4-NTP) solution with a final concentration of 10^{-5} M was added to Ag NPs-DNA conjugates and incubated for another 3 h at 4 °C, and the resultant solution was defined as DNA-NTP-Ag NPs. After the solution was then centrifuged (14 000 rpm, 30 min) at 4 °C, it was washed three times with 1× TAE-Mg^{2+} buffer to remove excess DNA and Raman reporters. The resulting products were redispersed in 1× TAE-Mg^{2+} buffer and stored at 4 °C until further use. On the basis of the literature,[46] the concentration of Ag NPs was calculated by UV−vis spectra.

Preparation of DNA Tweezers and DNA Tweezer-Ag NPs Probe. Unmodified DNA tweezers were fabricated by mixing strands T1−T9 and aptamer to a final concentration of 0.1 μM in 1× TAE-Mg^{2+} buffer. The temperature steps in the annealing protocol were listed in Table S2. For DNA tweezer-Ag NPs probe preparation, DNA-NTP functionalized Ag NPs (DNA-NTP-Ag NPs) and previously prepared DNA tweezers were mixed in a stoichiometric ratio of 2:1 in 1 × TAE-Mg^{2+} buffer and then incubated at 25 °C for 1.5 h. Subsequently, the product was centrifuged at 12 000 rpm at 4 °C for 30 min and washed three times using 1× TAE-Mg^{2+} buffer to remove excess DNA strands. The precipitation was redispersed in 1× TAE-Mg^{2+} buffer and stored at 4 °C until further use.

Agarose Gel Electrophoresis. The synthesis of DNA tweezers was evaluated by agarose gel electrophoresis. Specifically, 10 μL of 0.1 μM DNA tweezers sample was mixed with 2 μL of 6× commercial loading buffer. The mixtures were subjected to electrophoretic analysis on 2% agarose gel. The electrophoresis was performed in 1× TAE-Mg^{2+} under 180 V constant voltage for 30 min with an ice−water bath. The bands were stained with YeaRed nucleic acid gel staining dye and imaged using a ChemiDoc Touch gel imaging system.

AFM Imaging. Imaging was determined in ScanAsyst mode in air. Typically, 5 μL of 50 nM DNA sample was

https://dx.doi.org/10.1021/acs.analchem.9b04822
Anal. Chem. 2020, 92, 4900−4907

Scheme 1. Schematic Illustration of Detecting AFB_1 by the DNA Tweezer-Ag NPs Probe

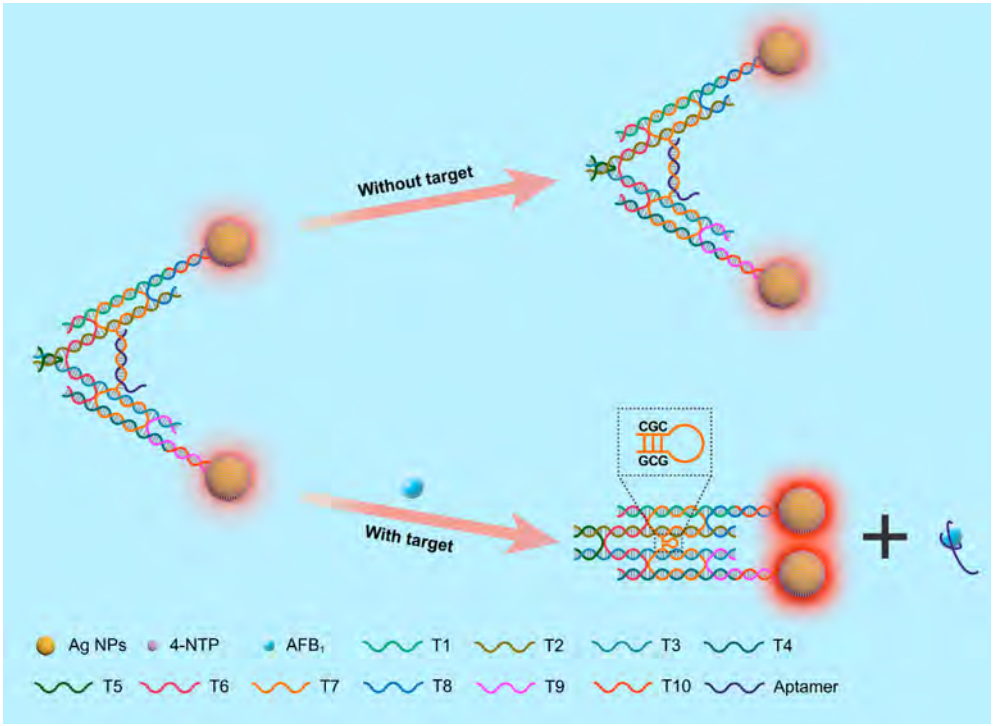

dropped on the freshly prepared mica surface. The sample was incubated for 2 min. After that 70 μL of 1× TAE-Mg^{2+} (12.5 mM) was added subsequently and incubated for an additional 5 min. Finally, the sample was rinsed with ultrapure water to remove salts and then dried by a stream of Argon before placing them in the AFM instrument for imaging.

Raman Measurement. For Raman detection, a portion of 10 μL of DNA tweezer-Ag NPs probe was mixed with 1 μL of different concentration of AFB_1 solution or artificial DNA strands. Then the mixture was incubated at 25 °C for 1 h. The resultant solution was sucked by a capillary (inner diameter ~1 mm) for Raman measurement. Raman spectroscopy was carried out under a 50× visible objective with a 633 nm laser radiation. The acquisition time was 10 s, and it was accumulated once. For each sample, five random spots were selected for collecting Raman spectra.

Food Sample Detection. Maize samples (~1.5 g) were first dried and fully comminuted. After adding 3 mL of 20% methanol aqueous solution, the mixture was ultrasonic extraction for 30 min and then centrifuged at 12 000 rpm for 20 min. The obtained supernatant was passed through a 0.22 μm filter to remove impurities. Finally, AFB_1 standard samples with various concentrations were added to the supernatant. The acquired samples were utilized as spike recovery samples and were detected by the above method. For certificated real foodstuffs, 84% acetonitrile aqueous solution was added to the sample and extracted on a shaker for 90 min. Then the obtained mixture solution was centrifuged at 6000 rpm for 20 min, and the obtained supernatant was passed through a 0.22 μm filter to remove impurities. The detection method was the same as that described above.

RESULTS AND DISCUSSION

Principle of DNA Tweezer-Actuated SERS Probe for AFB_1 Detection. The overall strategy of using DNA tweezer-actuated SERS probe for AFB_1 detection is shown in Scheme 1. The unmodified DNA tweezer with double-crossover motifs is adapted from a previous report with some modifications.[31,47] The single-stranded DNAs (T1-T9 and aptamer, listed in Table S1) are mixed and annealed on the basis of the procedure exhibited in Table S2 to form the open state DNA tweezer. Serving as a free component to regulate the state of the DNA tweezer, a 30-nucleotide single-stranded DNA (5′-TTTGCGAGACAACACGTGCCCAACCGCTTT-3′, T7-S) is incorporated in the middle of the designed T7 sequence and partially hybridized with the AFB_1 aptamer. The DNA is designed to form a stem-loop hairpin structure that allows the two cantilevers of the DNA tweezers to be clamped together by "GCG" hybridization.[31,47] This design can be used to amplify the small distance between the two back ends of the DNA tweezer into a larger dimensional change.[48] At the end of each tweezer arm, the 3′ end of the sequence T8 and the 5′ end of the sequence T9 each has an overhang DNA sequence that is complementary to the probe molecule modified at the interface of Ag NPs. The DNA tweezer and DNA-NTP-Ag NPs were hybridized in a ratio of 1:2 to form the final DNA tweezer-Ag NPs probe. In the absence of target (AFB_1), a longer gap length between Ag NPs is obtained, which causes a low Raman signal. Subsequently, following the addition of AFB_1, because of the specific biorecognition between the biomarker and its corresponding aptamer, the DNA tweeezer is closed and accompanied by showing a shorter gap length, which causes the increase of Raman signal.[36] Considering the distance of DNA tweezers, Ag NPs with a diameter of about 10 nm was chosen for the experiment. By monitoring the changes of the SERS signal, the target concentration is quantified using the activable DNA tweezer-Ag NPs probe.

Characterization of Ag NPs and DNA-NTP-Ag NPs. TEM was first performed to characterize the synthesized Ag NPs and DNA-NTP-Ag NPs. As shown in Figure 1a, Ag NPs

https://dx.doi.org/10.1021/acs.analchem.9b04822
Anal. Chem. 2020, 92, 4900−4907

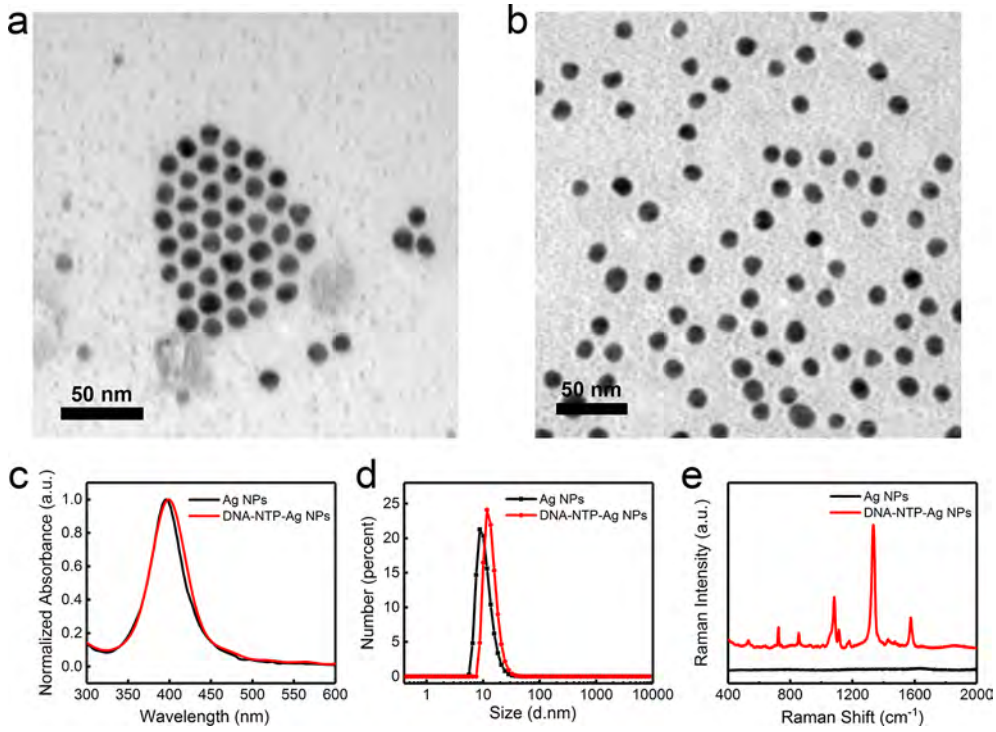

Figure 1. Characterization of Ag NPs and DNA-NTP-Ag NPs. TEM image of Ag NPs (a) and DNA-NTP-Ag NPs (b). UV−vis spectra (c), DLS (d), and Raman spectra (e) of Ag NPs and DNA-NTP-Ag NPs.

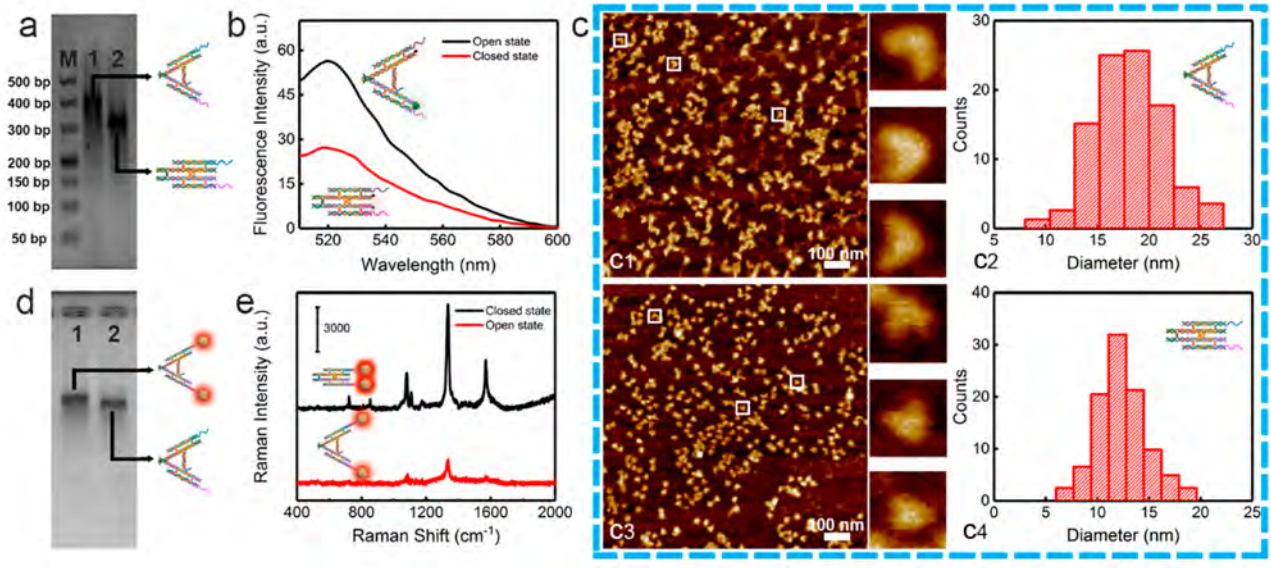

Figure 2. (a) 2% agarose gel electrophoresis of open (Lane 1) and closed (Lane 2) state of unmodified DNA tweezers. (b) FRET measurement experiment of open (black line) and closed (red line) DNA tweezers. (c) AFM image of open (c1) and closed (c3) DNA tweezers. The zoomed-in images of the tweezers are placed from top to bottom as they (highlighted by boxes) appear from left to right in the field of view. Statistical distribution of interarm distance for open tweezers (18.7 nm ±3.6 nm, c2) and closed tweezers (12.5 nm ±2.4 nm, c4). Scale bar: 100 nm (c1, c3). (d) Agarose gel electrophoresis of original (Line 2) and Ag NPs labeled (Line 1) DNA tweezers. (e) Raman spectra of closed (black) and open (red) state DNA tweezer-Ag NPs probe.

with an average diameter of ∼10 nm were successfully synthesized. After they were modified with SH-DNA (T10) and Raman reporter (4-NTP), the size and shape of the Ag NPs did not change significantly (Figure 1b), suggesting the modified Ag NPs were stable. The localized surface plasmon resonance (LSPR) band of Ag NPs showed a slight red shift from 396 to 399 nm after surface modification (Figure 1c), resulting from the sensitivity of LSPR for novel metal nanoparticles to the dielectric constant.[38,49] Figure 1d revealed that the hydration diameter of Ag NPs rose from 10.9 ± 3.7 nm to 13.9 ± 4.1 nm after conjugation with SH-DNA and Raman reporter. Figure 1e confirms the Ag NPs was successful modified by 4-NTP. As observed in Figure 1e, bare Ag NPs exhibited a neglectable Raman signal, while DNA-NTP-Ag NPs produced a strong Raman signal attributed to 4-NTP. The energy dispersive X-ray spectroscopy (EDS) analysis shows the

https://dx.doi.org/10.1021/acs.analchem.9b04822
Anal. Chem. 2020, 92, 4900−4907

elemental composition of the Ag NPs before and after modification (Figure S2). The EDS spectrum revealed the existence of C, Cu, Ag, O, Si, Al, Na, and S in Ag NPs (Figure S2a) and C, Cu, Ag, O, Si, Al, P, and S in DNA-NTP-conjugated Ag NPs (Figure S2b). The Ag elements came from the Ag NPs and P peak came from the DNA that was used in our modification. All these results suggested that SH-DNA and Raman reporter were successfully modified on the surface of Ag NPs.

Feasibility Test of Assay Protocol. To verify the successful self-assembly of unmodified DNA tweezer, an agarose gel electrophoresis experiment was performed. As can be seen from Figure 2a Lane 1, only one band can be clearly observed, indicating that the designed tweezers were successfully formed as expected and possessed high assembly efficiency. After adding the target (AFB_1), Lane 2 in Figure 2a had an obvious mobility shift. This phenomenon can be explained as follows: when the target was added, the aptamer specifically bound to the target, causing it to fall off from the DNA tweezer. Therefore, the conformation of the tweezer was more compact, leading to a slightly faster migration than the open state because the tweezer has a large steric hindrance when it is in an open state.[31,47,50] The result of gel electrophoresis preliminarily demonstrated the DNA tweezers in open and closed state. As shown in Figure 2b, the open and closed state of DNA tweezers were also characterized by a fluorescent resonance energy transfer (FRET) experiment (The end of T8 and T9 strands used here were modified with BHQ1 and FAM at the 5′ and 3′, respectively).[51] In the open state, the distance between FAM and BHQ1 are too large for efficient FRET, showing a significant fluorescence signal (black line).[29] When the target was added, the DNA tweezer was closed because of the specific binding of the aptamer and target. In this state, a decrease of fluorescence (red line) could be evidently observed, reflecting that the dyes on DNA tweezers were tightly closed resulting in efficient FRET. Then the DNA tweezers in open and closed state were characterized by atomic force microscope in Figure 2C. As shown in Figure 2c1 and Figure S3a, well-defined assemblies with two clear arms in open state can be observed. The DNA tweezers in open state displayed a distribution of distance between the two arms 18.7 nm ± 3.6 nm (Figure 2c2). When AFB_1 was added, the DNA tweezers became closed (Figure 2c3 and Figure S3b), and the distance between two arms reduced to 12.5 nm ±2.4 nm (Figure 2c4). Altogether, these results revealed that the designed DNA tweezer can respond to the target successfully.

Furthermore, we combined the DNA tweezer with Ag NPs for SERS detection of AFB_1. In order to realize our goal, we conjugated the above modified Ag NPs to the DNA tweezer (DNA tweezer-Ag NPs probe). As shown in Figure 2d, after incubating the unmodified DNA tweezer with DNA-NTP-Ag NPs, a much-slower-moving band (Lane 1, Figure 2d) than the DNA tweezer in the open state (Lane 2, Figure 2d), representing the DNA tweezer-Ag NPs complex, was clearly observed.[52] This result demonstrated the successful conjugation of DNA tweezer and modified Ag NPs. The LSPR band of DNA tweezer with Ag NPs was red-shifted after 10 nM AFB_1 was added (Figure S4). The red shift can be attributed to the formation of a new plasma coupling mode, which is sensitive to coupling strength. The coupling strength can be adjusted by the distance between the particles.[36,53] Figure S5 displayed the TEM images of open (Figure S5a) and closed (Figure S5b) DNA tweezer-Ag NPs probe. The formation of dimers was clearly observed from the image, which revealed the successful construction of the DNA tweezer-Ag NPs probe. Additionally, the distances between the two Ag NPs in open and closed state were 8.1 ± 2.7 nm and 3.2 ± 0.8 nm, respectively. Furthermore, SERS experiments were performed to demonstrate the open and closed state of DNA tweezer-Ag NPs probe. As shown in Figure 2e, in the absence of AFB_1, the Raman spectrum displayed a weak signal. However, with the addition of AFB_1, the Raman signal significantly enhanced because of the proximity of the two Ag NPs.[23,36,54] The SERS analytical enhancement factor (AEF) is also a major parameter for characterizing the SERS effect. According to eq 1 (SI), the AEF of DNA tweezer-Ag NPs probes in open and closed state were 2.20×10^5 (RSD = 6.3%) and 8.64×10^5 (RSD = 5.3%), respectively (details of the calculation shown in SI). All these results indicated that the DNA tweezer-Ag NPs probe was successfully fabricated and can be employed to detect AFB_1 in this study.

Optimization of the Activity of DNA Tweezer-Ag NPs Probe. In order to achieve the optimal biosensing performance, we optimized the incubation time and the length of the T7 linker. The concentration of AFB_1 used was 10 pg/mL. Raman intensity ratio of DNA tweezer-Ag NPs probe in closed and open state (I_{closed}/I_{open}) was used to evaluate the performance. First, the incubation time with the T7-S30 sequence was optimized. Figure 3a presents that with the

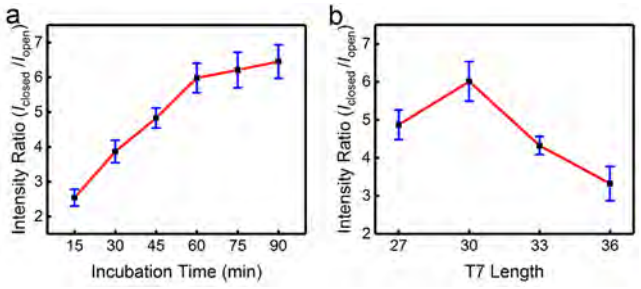

Figure 3. Optimization of incubation time (a) and T7 linker length (b) for DNA tweezer-Ag NPs probe activity.

increasing incubation time, the I_{closed}/I_{open} ratio increased and remained almost constant after 60 min. Therefore, 60 min was selected as the optimal incubation time. In addition, the length of T7-S has a vital impact on the Raman intensity because SERS intensity is closely related to the distance between nanoparticles.[55,56] To investigate the effect of T7 length, T7 sequences with varying lengths were employed. As shown in Figure 3b, it was found that the I_{closed}/I_{open} ratio reached the maximum value when the T7-S30 sequence was selected. Hence, the optimal T7 length was chosen as T7-S30 in the following experiment.

Detection of AFB_1. Until now, it turned out that the DNA tweezer-Ag NPs probe has been successfully prepared. The DNA tweezer-Ag NPs probe was then employed to detect AFB_1. Figure 4 shows the linear calibration plot between SERS spectra and different concentrations of AFB_1. As can be seen from Figure 4a, with the increasing AFB_1 concentration, the Raman intensity increased. Sackmann and Materny have revealed that the Raman intensity and the logarithmic concentration of target analytes follow a semilog linear regression.[57] In this study, a semilog linear model was employed to fit the date. Figure 4b shows the intensity of

https://dx.doi.org/10.1021/acs.analchem.9b04822
Anal. Chem. 2020, 92, 4900−4907

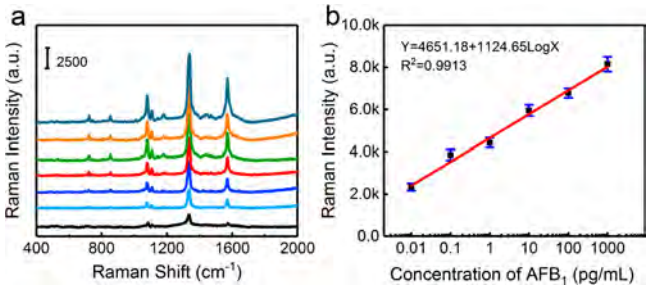

Figure 4. (a) SERS spectra of AFB_1 with concentrations of 1000, 100, 10, 1, 0.1, 0.01, and 0 pg/mL from top to bottom. (b) Linear calibration plot between the SERS intensity and the logarithmic AFB_1 concentration. Error bars in (b) show the standard deviation of five experiments.

Raman peak at 1334 cm^{-1} and linear calibration plot of different logarithmic concentration of AFB_1. The linear regression equation was $Y = 4651.18 + 1124.65\text{Log}X$ and the correlation coefficient (R^2) was 0.9913. The X value is the concentration of AFB_1, and the Y value is the intensity of Raman peak at 1334 cm^{-1}.

The limit of detection (LOD) is calculated to verify the sensitivity of DNA tweezer-Ag NPs probe. Details of the calculation were described in Supporting Information. According to the signal-to-noise ratio defined by the International Union of Pure and Applied Chemistry (IUPAC),[58] the LOD of DNA tweezer-Ag NPs probe for AFB_1 was calculated to be 5.07 fg/mL. Impressively, the proposed method exhibits higher sensitivity for detecting AFB_1 than most of the results reported in the literature as shown in Table 1, indicating the DNA tweezer-Ag NPs probe has excellent biosensing performance.

Table 1. Comparison of the Limit of Detection (LOD) of Different Methods for AFB_1 Detection

no.	analytical methods	LOD (g/mL)	ref
1	ECL	3.9×10^{-12}	59
2	PEC	2.0×10^{-12}	60
3	fluorescent	5.0×10^{-12}	61
4	RT-qPCR-based aptasensor	2.5×10^{-14}	62
5	EIS	1.5×10^{-11}	63
6	electrochemical	0.4×10^{-10}	64
7	electrochemical	1.8×10^{-14}	65
8	SERS	4.1×10^{-16}	49
9	SERS	0.3×10^{-10}	45
10	SERS	5.1×10^{-15}	this work

In addition, the recovery of AFB_1 in maize samples is presented in Table S5. After adding different concentrations of AFB_1 into corn samples, the recovery rate of AFB_1 was in the range of 95.6−106.4% (as shown in Table S5). The results verified that the DNA tweezer-Ag NPs probe was acceptable in practical applications. In order to provide more sufficient evidence to prove the application of the DNA tweezer-Ag NPs probe in real situation, certificated real foodstuffs (corn powder samples) were used. The result was shown in Table S6. The results indicated that the DNA tweezer-Ag NPs probe developed in this study can be regarded as a sensitive and effective SERS biosensor for detecting AFB_1 in real food samples.

Additionally, we also demonstrated the feasibility to detect oligonucleotide using the proposed DNA tweezer-Ag NPs probe. As shown in Figure S6a, with the decreasing concentration of complementary oligonucleotide (T11), the Raman intensity decreased. Figure S6b shows the linear calibration plot between the intensity of Raman peak at 1334 cm^{-1} and the logarithmic concentration of complementary oligonucleotide. Furthermore, the linear regression equation was $Y = 8839.89 + 2286.98\text{Log}X$ with the correlation coefficient R^2 of 0.9892, and the LOD of complementary oligonucleotide was 1.1 fM. This result indicated our DNA tweezer-Ag NPs probe have programmability and versatility for sensitive detection of a variety of targets.

Selectivity of AFB_1. The selectivity of the proposed biosensor was investigated in the presence of nonspecific molecules, including AFB_2, AFG_1, AFG_2, AFM_1, ZON, DON and the control groups without any targets. As illustrated in Figure 5, despite the concentration of interference species

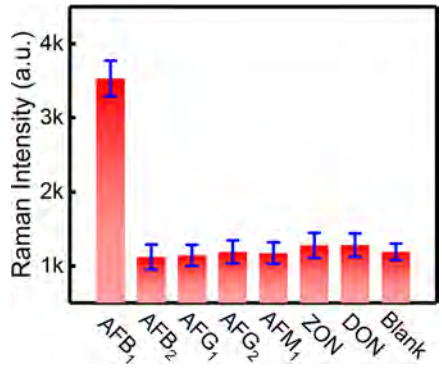

Figure 5. Specificity analysis of the biosensor to AFB_1, AFB_2, AFM_1, AFG_1, AFG_2, ZON, and DON. The concentration of AFB_1 was 0.1 pg/mL, and that of other samples was 10 pg/mL. Error bars show the standard deviation of three experiments.

being 100-fold higher than AFB_1, no obvious SERS signal changes were observed compared to the blank. In comparison, a significant SERS signal enhancement displayed in the presence of AFB_1 at a concentration of 0.1 pg/mL. The results confirmed that the DNA tweezer-Ag NPs probe had a perfect selectivity to AFB_1 due to the favorable bioaffinity of aptamers.

CONCLUSIONS

In summary, an aptamer-based DNA tweezer-Ag NPs SERS probe with significant specificity for the detecting AFB_1 was successfully developed. The specific biorecognition between the AFB_1 and the given aptamer ensured the specificity and sensitivity of the method. The LOD for AFB_1 was 5.07 fg/mL with a linear range from 1 ng/mL to 0.01 pg/mL. In addition, this method showed high specificity to AFB_1 compared with six common mycotoxins. Moreover, this method exhibited excellent performance in spike recovery and real food samples. All these results showed that this protocol may be used as a promising technology for detection of mycotoxins and small molecules in the future.

ASSOCIATED CONTENT

Supporting Information

The Supporting Information is available free of charge at https://pubs.acs.org/doi/10.1021/acs.analchem.9b04822.

https://dx.doi.org/10.1021/acs.analchem.9b04822
Anal. Chem. 2020, 92, 4900−4907

Oligonucleotides sequences of DNA tweezers in the experiment; design of DNA tweezer; thermal annealing program for DNA tweezers; EDS analysis of Ag NPs and DNA-NTP-Ag NPs; AFM image of large field DNA tweezers in different state; normalized extinction spectra of DNA tweezer-Ag NPs probe in the absence and that in the presence of 10 nM AFB_1; TEM of DNA tweezer-Ag NPs probe in different state; AEF calculation of the DNA tweezer-Ag NPs probe in open and closed state; calculation of the LOD of AFB_1; recovery of AFB_1 spiked in maize samples; validated results for real-life maize specimens from SPE and DNA tweezer-Ag NPs probe (PDF)

AUTHOR INFORMATION

Corresponding Author

Heyou Han − *State Key Laboratory of Agricultural Microbiology, College of Food Science and Technology and State Key Laboratory of Agricultural Microbiology, College of Science, Huazhong Agricultural University, Wuhan, Hubei 430070, People's Republic of China;* orcid.org/0000-0001-9406-0722; Email: hyhan@mail.hzau.edu.cn

Authors

Jinjie Li − *State Key Laboratory of Agricultural Microbiology, College of Food Science and Technology, Huazhong Agricultural University, Wuhan, Hubei 430070, People's Republic of China*

Wenjing Wang − *State Key Laboratory of Agricultural Microbiology, College of Science, Huazhong Agricultural University, Wuhan, Hubei 430070, People's Republic of China;* orcid.org/0000-0003-4035-8552

Hao Zhang − *State Key Laboratory of Agricultural Microbiology, College of Science, Huazhong Agricultural University, Wuhan, Hubei 430070, People's Republic of China*

Zhicheng Lu − *State Key Laboratory of Agricultural Microbiology, College of Science, Huazhong Agricultural University, Wuhan, Hubei 430070, People's Republic of China*

Wenxin Wu − *State Key Laboratory of Agricultural Microbiology, College of Science, Huazhong Agricultural University, Wuhan, Hubei 430070, People's Republic of China*

Mingbo Shu − *State Key Laboratory of Agricultural Microbiology, College of Science, Huazhong Agricultural University, Wuhan, Hubei 430070, People's Republic of China*

Complete contact information is available at: https://pubs.acs.org/10.1021/acs.analchem.9b04822

Author Contributions

§J.L. and W.W. contributed equally.

Notes

The authors declare no competing financial interest.

ACKNOWLEDGMENTS

We gratefully acknowledge the financial support from Science and Technology Major Project of Guangxi (Gui Ke AA18118046), National Key R&D Program of China (2016YFD0500706), National Natural Science Foundation of China (21804046, 21778020), Sci-tech Innovation Foundation of Huazhong Agriculture University (2662017PY042, 2662018PY024), and Fundamental Research Funds for the Central Universities (2662018QD012).

REFERENCES

(1) Seeman, N. C. *Mol. Biotechnol.* **2007**, *37*, 246−57.
(2) Rothemund, P. W. K. *Nature* **2006**, *440*, 297−302.
(3) Kuzyk, A.; Jungmann, R.; Acuna, G. P.; Liu, N. *ACS Photonics* **2018**, *5*, 1151−1163.
(4) Schuller, J. A.; Barnard, E. S.; Cai, W.; Jun, Y. C.; White, J. S.; Brongersma, M. L. *Nat. Mater.* **2010**, *9*, 193−204.
(5) Cardinal, M. F.; Vander Ende, E.; Hackler, R. A.; McAnally, M. O.; Stair, P. C.; Schatz, G. C.; Van Duyne, R. P. *Chem. Soc. Rev.* **2017**, *46*, 3886−3903.
(6) Schlücker, S. *Angew. Chem., Int. Ed.* **2014**, *53*, 4756−4795.
(7) Xu, L. J.; Lei, Z. C.; Li, J.; Zong, C.; Yang, C. J.; Ren, B. *J. Am. Chem. Soc.* **2015**, *137*, 5149−5154.
(8) Sprague-Klein, E. A.; Negru, B.; Madison, L. R.; Coste, S. C.; Rugg, B. K.; Felts, A. M.; McAnally, M. O.; Banik, M.; Apkarian, V. A.; Wasielewski, M. R.; Ratner, M. A.; Seideman, T.; Schatz, G. C.; Van Duyne, R. P. *J. Am. Chem. Soc.* **2018**, *140*, 10583−10592.
(9) Wu, Z.; Liu, Y.; Zhou, X.; Shen, A.; Hu, J. *Biosens. Bioelectron.* **2013**, *44*, 10−15.
(10) Wang, K.; Sun, D. W.; Pu, H.; Wei, Q.; Huang, L. *ACS Appl. Mater. Interfaces* **2019**, *11*, 29177−29186.
(11) Wang, K.; Sun, D. W.; Pu, H.; Wei, Q. *Talanta* **2019**, *191*, 449−456.
(12) Nie, S.; Emory, S. R. *Science* **1997**, *275*, 1102−1106.
(13) Zhang, H.; Wang, C.; Sun, H. L.; Fu, G.; Chen, S.; Zhang, Y. J.; Chen, B. H.; Anema, J. R.; Yang, Z. L.; Li, J. F.; Tian, Z. Q. *Nat. Commun.* **2017**, *8*, 15447.
(14) Fang, W.; Zhang, X.; Chen, Y.; Wan, L.; Huang, W.; Shen, A.; Hu, J. *Anal. Chem.* **2015**, *87*, 9217−9224.
(15) Li, Y.; Gao, T.; Xu, G.; Xiang, X.; Zhao, B.; Han, X. X.; Guo, X. *Anal. Chem.* **2019**, *91*, 7980−7984.
(16) Chen, Y.; Ren, J. Q.; Zhang, X. G.; Wu, D. Y.; Shen, A. G.; Hu, J. M. *Anal. Chem.* **2016**, *88*, 6115−6119.
(17) Li, J. F.; Tian, X. D.; Li, S. B.; Anema, J. R.; Yang, Z. L.; Ding, Y.; Wu, Y. F.; Zeng, Y. M.; Chen, Q. Z.; Ren, B.; Wang, Z. L.; Tian, Z. Q. *Nat. Protoc.* **2013**, *8*, 52−65.
(18) Shen, B.; Kostiainen, M. A.; Linko, V. *Langmuir* **2018**, *34*, 14911−14920.
(19) Thacker, V. V.; Herrmann, L. O.; Sigle, D. O.; Zhang, T.; Liedl, T.; Baumberg, J. J.; Keyser, U. F. *Nat. Commun.* **2014**, *5*, 3448.
(20) Heck, C.; Prinz, J.; Dathe, A.; Merk, V.; Stranik, O.; Fritzsche, W.; Kneipp, J.; Bald, I. *ACS Photonics* **2017**, *4*, 1123−1130.
(21) Zhan, P.; Wen, T.; Wang, Z. G.; He, Y.; Shi, J.; Wang, T.; Liu, X.; Lu, G.; Ding, B. *Angew. Chem., Int. Ed.* **2018**, *57*, 2846−2850.
(22) Prinz, J.; Heck, C.; Ellerik, L.; Merk, V.; Bald, I. *Nanoscale* **2016**, *8*, 5612−5620.
(23) Ding, S. Y.; Yi, J.; Li, J. F.; Ren, B.; Wu, D. Y.; Panneerselvam, R.; Tian, Z. Q. *Nat. Rev. Mater.* **2016**, *1*, 16021.
(24) Wang, K.; Sun, D. W.; Pu, H.; Wei, Q. *Food Chem.* **2020**, *310*, 125923.
(25) Heck, C.; Kanehira, Y.; Kneipp, J.; Bald, I. *Angew. Chem., Int. Ed.* **2018**, *57*, 7444−7447.
(26) Yurke, B.; Turberfield, A. J.; Mills, A. P.; Simmel, F. C.; Neumann, J. L. *Nature* **2000**, *406*, 605−608.
(27) Yang, W.; Shen, Y.; Zhang, D.; Li, C.; Yuan, R.; Xu, W. *Anal. Chem.* **2019**, *91*, 7782−7789.
(28) Bian, X.; Guo, B.; Zhao, M.; Han, D.; Cheng, W.; Song, F.; Ding, S. *ACS Appl. Mater. Interfaces* **2019**, *11*, 3715−3721.
(29) Xu, X.; Wang, L.; Li, K.; Huang, Q.; Jiang, W. *Anal. Chem.* **2018**, *90*, 3521−3530.
(30) Zeng, S.; Liu, D.; Li, C.; Yu, F.; Fan, L.; Lei, C.; Huang, Y.; Nie, Z.; Yao, S. *Anal. Chem.* **2018**, *90*, 13459−13466.
(31) Liu, M.; Fu, J.; Hejesen, C.; Yang, Y.; Woodbury, N. W.; Gothelf, K.; Liu, Y.; Yan, H. *Nat. Commun.* **2013**, *4*, 2127.
(32) Xin, L.; Zhou, C.; Yang, Z.; Liu, D. *Small* **2013**, *9*, 3088−3091.
(33) Kou, B.; Chai, Y.; Yuan, Y.; Yuan, R. *Anal. Chem.* **2018**, *90*, 10701−10706.
(34) Rushing, B. R.; Selim, M. I. *Food Chem. Toxicol.* **2019**, *124*, 81−100.

(35) Wu, L.; Li, G.; Xu, X.; Zhu, L.; Huang, R.; Chen, X. *TrAC, Trends Anal. Chem.* **2019**, *113*, 140−156.
(36) Xu, L.; Yan, W.; Ma, W.; Kuang, H.; Wu, X.; Liu, L.; Zhao, Y.; Wang, L.; Xu, C. *Adv. Mater.* **2015**, *27*, 1706−1711.
(37) Liu, Y.; Huang, C. Z. *Analyst* **2012**, *137*, 3434−3436.
(38) Zhang, X.; Servos, M. R.; Liu, J. *Chem. Commun.* **2012**, *48*, 10114−10116.
(39) Dhakal, S.; Adendorff, M. R.; Liu, M.; Yan, H.; Bathe, M.; Walter, N. G. *Nanoscale* **2016**, *8*, 3125−3137.
(40) Xing, C.; Huang, Y.; Dai, J.; Zhong, L.; Wang, H.; Lin, Y.; Li, J.; Lu, C. H.; Yang, H. H. *ACS Appl. Mater. Interfaces* **2018**, *10*, 32579−32587.
(41) Tang, H.; Meng, G.; Huang, Q.; Zhang, Z.; Huang, Z.; Zhu, C. *Adv. Funct. Mater.* **2012**, *22*, 218−224.
(42) Shen, W.; Lin, X.; Jiang, C.; Li, C.; Lin, H.; Huang, J.; Wang, S.; Liu, G.; Yan, X.; Zhong, Q.; Ren, B. *Angew. Chem., Int. Ed.* **2015**, *54*, 7308−7312.
(43) Lee, P.; Meisel, D. *J. Phys. Chem.* **1982**, *86*, 3391−3395.
(44) Si, Y.; Bai, Y.; Qin, X.; Li, J.; Zhong, W.; Xiao, Z.; Li, J.; Yin, Y. *Anal. Chem.* **2018**, *90*, 3898−3905.
(45) Zhao, Y.; Yang, Y.; Luo, Y.; Yang, X.; Li, M.; Song, Q. *ACS Appl. Mater. Interfaces* **2015**, *7*, 21780−21786.
(46) Paramelle, D.; Sadovoy, A.; Gorelik, S.; Free, P.; Hobley, J.; Fernig, D. G. *Analyst* **2014**, *139*, 4855−4861.
(47) Zhou, C.; Yang, Z.; Liu, D. *J. Am. Chem. Soc.* **2012**, *134*, 1416−1418.
(48) Liu, M.; Jiang, S.; Loza, O.; Fahmi, N. E.; Sulc, P.; Stephanopoulos, N. *Angew. Chem., Int. Ed.* **2018**, *57*, 9341−9345.
(49) Li, Q.; Lu, Z.; Tan, X.; Xiao, X.; Wang, P.; Wu, L.; Shao, K.; Yin, W.; Han, H. *Biosens. Bioelectron.* **2017**, *97*, 59−64.
(50) Meng, H. M.; Liu, H.; Kuai, H.; Peng, R.; Mo, L.; Zhang, X. B. *Chem. Soc. Rev.* **2016**, *45*, 2583−2602.
(51) Han, X.; Zhou, Z.; Yang, F.; Deng, Z. *J. Am. Chem. Soc.* **2008**, *130*, 14414−14415.
(52) Zheng, Y.; Li, Y.; Deng, Z. *Chem. Commun.* **2012**, *48*, 6160−6162.
(53) Yuan, P.; Ma, R.; Guan, Z.; Gao, N.; Xu, Q. H. *ACS Appl. Mater. Interfaces* **2014**, *6*, 13149−13156.
(54) Lim, D. K.; Jeon, K. S.; Kim, H. M.; Nam, J. M.; Suh, Y. D. *Nat. Mater.* **2010**, *9*, 60−67.
(55) Li, J.; Yan, H.; Tan, X.; Lu, Z.; Han, H. *Anal. Chem.* **2019**, *91*, 3885−3892.
(56) Zong, C.; Xu, M.; Xu, L. J.; Wei, T.; Ma, X.; Zheng, X. S.; Hu, R.; Ren, B. *Chem. Rev.* **2018**, *118*, 4946−4980.
(57) Sackmann, M.; Materny, A. *J. Raman Spectrosc.* **2006**, *37*, 305−310.
(58) IUPAC. *Compendium of Chemical Terminology—The "Gold Book"*, 2nd ed.; Blackwell Scientific Publications: Oxford, 1997.
(59) Wang, Y.; Zhao, G.; Li, X.; Liu, L.; Cao, W.; Wei, Q. *Biosens. Bioelectron.* **2018**, *101*, 290−296.
(60) Zhang, B.; Lu, Y.; Yang, C.; Guo, Q.; Nie, G. *Biosens. Bioelectron.* **2019**, *134*, 42−48.
(61) Wang, B.; Chen, Y.; Wu, Y.; Weng, B.; Liu, Y.; Lu, Z.; Li, C. M.; Yu, C. *Biosens. Bioelectron.* **2016**, *78*, 23−30.
(62) Guo, X.; Wen, F.; Zheng, N.; Luo, Q.; Wang, H.; Wang, H.; Li, S.; Wang, J. *Biosens. Bioelectron.* **2014**, *56*, 340−344.
(63) Wang, C.; Qian, J.; An, K.; Ren, C.; Lu, X.; Hao, N.; Liu, Q.; Li, H.; Huang, X.; Wang, K. *Biosens. Bioelectron.* **2018**, *108*, 69−75.
(64) Krittayavathananon, A.; Sawangphruk, M. *Anal. Chem.* **2017**, *89*, 13283−13289.
(65) Ge, J.; Zhao, Y.; Li, C.; Jie, G. *Anal. Chem.* **2019**, *91*, 3546−3554.

https://dx.doi.org/10.1021/acs.analchem.9b04822
Anal. Chem. 2020, 92, 4900−4907